Impaired hippocampal functions underlying memory encoding and consolidation precede robust Aβ deposition in a mouse model of Alzheimer's disease

Hanyan Li [1,2,#], Zhuoyang Zhao [1,2,#], Aline Fassini [1,2], Han K. Lee [1,2], Reese J. Green [1,2], and Stephen N. Gomperts [1,2,*]

[1] Department of Neurology, Massachusetts General Hospital, Boston, Massachusetts, USA.

[2] Harvard Medical School, Boston, Massachusetts, USA.

# Contributed equally to this work

* Correspondence: Gomperts.stephen@mgh.harvard.edu

Abstract

Current therapeutic strategies for Alzheimer's disease (AD) target amyloid-beta (Aβ) fibrils and high molecular weight protofibrils associated with plaques, but molecular cascades associated with AD may drive neural systems failure before Aβ plaque deposition in AD. Employing hippocampal electrophysiological recordings and dynamic calcium imaging across the sleep-wake cycle in the APP/PS1 mouse model of AD before Aβ plaques accumulated, we detected marked impairments of hippocampal systems function: In a spatial behavioral task, but not REM sleep, phase-amplitude coupling (PAC) of the hippocampal theta and gamma oscillations was impaired and place cell calcium fluctuations were hyper-synchronized with the theta oscillation. In subsequent slow wave sleep (SWS), place cell reactivation was reduced. These degraded neural functions underlying memory encoding and consolidation support targeting pathological processes of the pre-plaque phase of AD to treat and prevent hippocampal impairments.

Introduction

In Alzheimer's disease (AD), deposition of amyloid-beta42 (Aβ) in amyloid plaques and aggregation of intracellular tau in neurofibrillary tangles are associated with neuronal loss and progressive memory impairment on the basis of hippocampal systems failure (1). The advent of amyloid-targeted immunotherapies such as Lecanemab (targeting high molecular weight Aβ protofibrils as well as fibrils in plaques) (2), Donanemab (targeting the pyroglutamate modification seen in Aβ fibrils in plaques) (3), and Aducanumab (targeting Aβ fibrils in plaques) (4) for the treatment of AD heralds the beginning of a new era, with evidence to date demonstrating marked reductions of brain amyloid. Even so, these treatments as yet have only modestly improved cognitive outcomes of AD patients (2,3,5). Several plausible explanations may explain this discrepancy, including the possibility of problems with the timing or molecular targets of these state-of-the-art treatments against neurodegeneration in AD.

Hippocampal functions are diffusely disrupted in Aβ plaque-laden mice such as the APPswe/PS1dE9 (APP/PS1) transgenic model that harbors genetic mutations that drive production of the Aβ42 peptide and cause autosomal dominant AD (6,7). During online memory encoding processes, hippocampal place cells form place fields that are activated sequentially as animals explore an environment in coordination with the hippocampal theta oscillation (8,9). In Aβ plaque-laden mice, place representations (10,11) and the coupling of the amplitude of gamma oscillations to the phase of theta (12–19) are impaired, and neuronal calcium fluctuations hyper-synchronize with the theta oscillation (20). Aβ plaque-laden mice also show impaired off-line hippocampal memory consolidation processes: In SWS, reduced reactivation of hippocampal place cell pairs (21) and reduced coordination of hippocampal sharp wave ripples (SWRs) with cortical spindles

53 and slow oscillations (20,22); in REM sleep, the same oscillatory impairments seen in wakefulness,
54 namely, reduced theta-gamma coupling (20,23,24), and hyper-synchronization of neuronal
55 calcium fluctuations with theta (20).
56
57 As some molecular species arising from aberrant degradation of the amyloid precursor protein
58 (APP) have been found to be cytotoxic (25), including soluble Aβ oligomers (AβO) that impair
59 synapse function, plasticity, and density (26–36) and have been found to drive hippocampal
60 neuronal hyper-excitability in anesthetized AD models (37–39) , we hypothesized that
61 impairments of hippocampal systems functions underlying memory encoding and consolidation
62 would be evident in advance of plaque deposition. To test this hypothesis, here we acquired
63 hippocampal dynamic calcium imaging and hippocampal and cortical electrophysiological
64 recordings across behavioral states in freely-behaving APP/PS1 transgenic mice in the window
65 before robust plaque deposition (6,40). We found marked impairments of hippocampal functions
66 underlying memory encoding and consolidation processes despite minimal Aβ plaque burden.
67
68 **Results**
69 To evaluate hippocampal function before plaque deposition, we acquired hippocampal CA1
70 dynamic calcium imaging with GCaMP6f using the Inscopix miniscope™ together with
71 simultaneous cortical and hippocampal local field potential (LFP) recordings of young APP/PS1
72 mice (5.2 ± 0.6 months, n=8, male) and their littermate controls (4.7 ± 0.5 months, n=7, male; age,
73 $p > 0.05$, 2-sided t-test), as animals explored a linear track (RUN), subsequently quiet wakefulness
74 (QW), slow wave sleep (SWS) and REM sleep in the home cage (Fig. 1a). Recording lengths of
75 each state were comparable between genotypes (Fig. S1).

Minimal burden of Aβ plaques and abundant soluble Aβ oligomers in young APP/PS1 mice

In the APP/PS1 model, Aβ plaques have been reported to first deposit around 6 months, with dense accumulation by 12 months (6,40). In line with these reports, we observed minimal deposition of Aβ plaques in hippocampus and cortex in young APP/PS1 mice, in contrast to 12-month-old mice (hippocampus: repeated measures ANOVA $F(4,15)=42.1$, $p<0.001$, post hoc comparison with positive control $p<0.001$; cortex: repeated measures ANOVA $F(4,15)=105.4$, $p<0.001$, post hoc comparison with positive control $p<0.001$, Fig. 1b, c). Soluble AβOs were detected in both hippocampus and cortex and increased with age (hippocampus $R=0.5$, $p=0.03$; cortex $R=0.6$, $p=0.006$, Pearson correlations, Fig. 1d, consistent with prior results (41,42)).

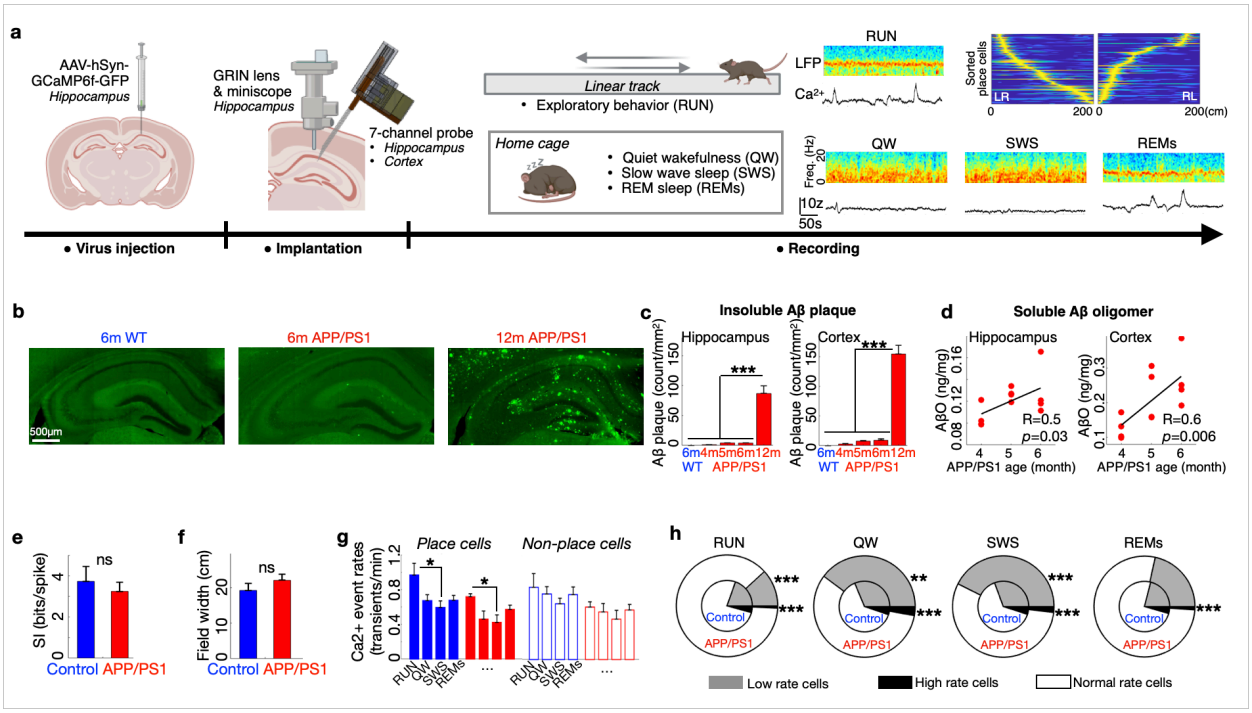

Figure 1. Young APP/PS1 mice expressing minimal Aβ plaque burden and abundant soluble AβO showed preserved place cell function and no calcium hyperactivity across the sleep-wake cycle. a) *Schematic of hippocampal calcium imaging and simultaneous ipsilateral LFP recording across the sleep-wake cycle: exploratory behavior (RUN), insert: examples of LFP spectrogram*

and one calcium trace across behavioral states; and examples of place cells sorted by their place fields (in yellow) in inbound (LR) and outbound (RL) directions. Yellow shows the place field of each cell; quiet wakefulness (QW); slow wave sleep (SWS) and rapid eye movement (REM) sleep. ***b)*** *Immunohistochemistry against Aβ in hippocampus of a wild-type control mouse (6 months) and APP/PS1 mice at 6 and 12 months. Green: Aβ plaques (D54D2).* ***c)*** *Aβ plaque counts in hippocampus and cortex were low in 4-6 month-old APP/PS1 mice and increased markedly at 12 months.* ***d)*** *Levels of soluble AβO in hippocampus and cortex increased with age in APP/PS1 mice.* ***e)*** *Spatial information (SI) and* ***f)*** *place field width were comparable across genotypes.* ***g)*** *Calcium event rates of place cells and non place cells in each behavioral state were similar to those of littermate control mice, and calcium event rates of place cells were higher in RUN than SWS in both genotypes.* ***h)*** *In RUN and REM sleep, APP/PS1 had fewer low rate and high rate cells; In QW and SWS, APP/PS1 had more low rate cells and fewer high rate cells. * p<0.05, ** p<0.01, ***p<0.001; c, g, ANOVA with post-hoc comparisons; e, f, 2-sided t-test; d, Pearson correlation; h, mixed effects model. b-d: each group n=4 mice; e-h: Control n=5 mice, 395 place cells, 2169 total cells; APP/PS1 n=6 mice, 237 place cells, 2133 total cells. Data are represented as mean ± S.E.M.*

Intact place representations but reduced dynamic calcium activity in quiet wakefulness and slow wave sleep before plaque deposition

Behavior was comparable across young APP/PS1 and littermate control groups, with similar run velocity (Control: 4.1 ± 0.7 cm/s; APP/PS1: 3.5 ± 0.6 cm/s, p>0.05, 2-sided t-test) and laps on the track (Control: 34.2 ± 3.2 laps; APP/PS1: 39.8 ± 2.5 laps, p>0.05, 2-sided t-test), consistent with prior reports (43).

To investigate place cell representations across the genotypes, which are often directional (44), we considered inbound (LR) and outbound (RL) trajectories separately (Fig. 1a insert). The proportion of place cells was similar in young APP/PS1 and control mice (Control: 16.8% ± 1.9%; APP/PS1: 11.0% ± 2.1%. p=0.07, 2-sided t-test). Spatial information (p>0.05, 2-sided t-test, Fig. 1e) and place field width (p>0.05, 2-sided t-test, Fig. 1f) were also similar across the genotypes. These results are consistent with prior work (45).

Previous studies in plaque-laden AD models have detected aberrant neuronal activity (20,37,38), and studies in young anesthetized AD mice (37,39) have reported hyperactivity of hippocampal neurons before amyloid plaque formation. We therefore extended analyses of neuronal activity of young APP/PS1 mice across the sleep-wake cycle, free from the complex effects of anesthesia (39). Unexpectedly, place cell and nonplace cell mean calcium event rates in each behavioral state of young APP/PS1 mice were similar to those of littermate control mice ($p>0.05$, 2-sided t-tests, Fig. 1g). We found no hyperactivity (defined as calcium event rates > 2SD above the control group mean (20)) in any behavioral state (high rate cell proportions, Control vs APP/PS1, RUN: 4.2% ± 0.4% vs 0.7% ± 0.6%, $p<0.001$; QW: 5.1% ± 0.4% vs 2.8% ± 1.9%, $p=0.001$; SWS: 4.9% ± 0.3% vs 1.8% ± 1.5%, $p<0.001$; REM sleep: 4.4% ± 0.5% vs 1.0% ± 0.8%, $p<0.001$. Mixed effects model, Fig 1h). Instead, we observed an increased proportion of hypoactive cells (< 0.25 spikes/min (20,37)) in APP/PS1 mice in QW and SWS (low rate cell proportions, Control vs APP/PS1, RUN: 19.5% ± 8.2% vs 11.7% ± 1.5%, $p<0.001$; QW: 31.2% ± 4.7% vs 39.8% ± 5.8%, $p=0.009$; SWS: 30.6% ± 3.5% vs 42.5% ± 11.5%, $p<0.001$; REM sleep: 21.0% ± 4.0% vs 21.5% ± 3.5%, ns. Mixed effects model, Fig 1h), regardless of place cell identity.

Consistent with prior results in plaque-laden APP/PS1 mice (20) (but see (39)), calcium event rates of place cells were higher in RUN than in SWS in both APP/PS1 and control mice (Control: repeated measures ANOVA: $F(3,16)=3.46$, $p=0.04$, post hoc comparison: RUN vs SWS, $p=0.03$; APP/PS1: repeated measures ANOVA: $F(3,20)=3.57$, $p=0.03$, post hoc comparison: RUN vs SWS, $p=0.003$, Fig. 1g). In both APP/PS1 and control mice, the calcium event rates of non-place cells were similar across behavioral states.

146 **Reduced place cell pairwise reactivation despite intact slow wave sleep oscillations before**
147 **robust plaque deposition**

148 Since place cell properties of young APP/PS1 mice were essentially intact at the single cell level,
149 we next evaluated place cell coordination in offline behavioral states. Place cells with overlapping
150 place fields during spatial behavioral tasks tend to fire together during subsequent rest and sleep
151 in the service of memory consolidation (46–48), and prior work has found that reactivation of place
152 cell pairs in SWS is reduced in Aβ plaque-bearing mice (21). We therefore set out to evaluate
153 whether place cell reactivation is perturbed prior to robust Aβ plaque deposition. SWR frequency
154 and duration in SWS were comparable in APP/PS1 and control mice (SWR rate: Control 0.061 ±
155 0.014 event/s; APP/PS1 0.089 ± 0.020 event/s; duration: Control 0.024 ± 0.0005 s; APP/PS1 0.025
156 ± 0.0006 s; $p>0.05$, 2-sided t-tests). We calculated the spike time cross-correlation of all place cell
157 pairs during exploratory behavior (RUN) and in subsequent offline states, and identified
158 reactivation when a place cell pair was coactive in both online and offline states (48) (Fig. 2a, see
159 Methods and Fig. S2). Pairwise reactivation was detected in each genotype by comparing to the
160 distribution of 500 cross-correlations of shuffled spike times (Supplementary Fig. S3a). The
161 percentage of place cell pairs that reactivated in SWS was significantly reduced in APP/PS1
162 compared to control mice ($p=0.005$, $T=3.6$, $df=9$, 2-sided t-test, Fig. 2a, b). Place cell activity and
163 numbers were comparable in APP/PS1 and control mice (see above), and this difference persisted
164 after matching place cell event rate and place cell numbers in control mice and APP/PS1 mice
165 (Supplementary Fig. S3b-d). In contrast to SWS, pairwise reactivation of APP/PS1 and control
166 mice was comparable in QW (as well as in REM sleep) ($p>0.05$, 2-sided t-test, Fig 2a, b). Thus,
167 hippocampal reactivation of place cell pairs in SWS was reduced in APP/PS1 mice prior to robust
168 Aβ plaque deposition.

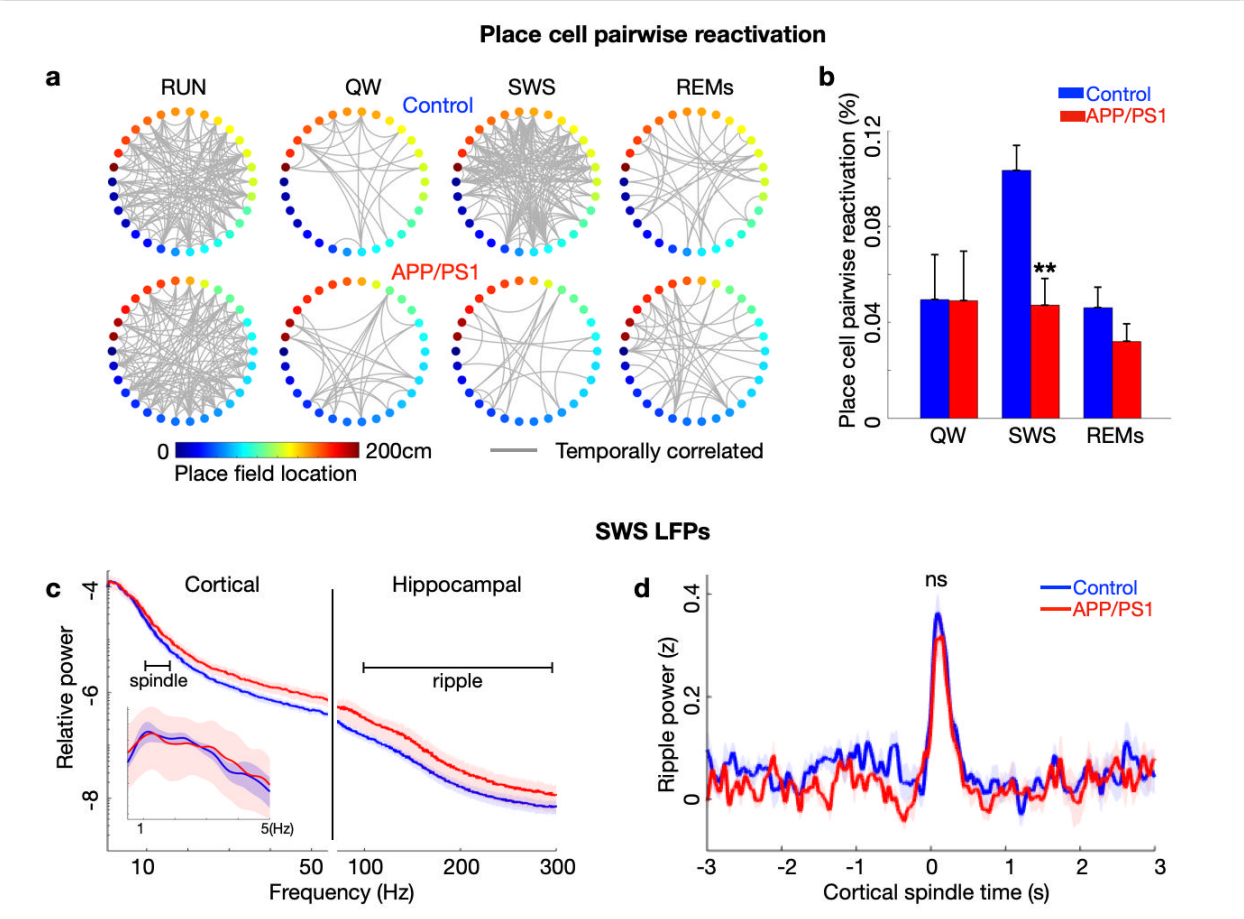

Figure 2. Young APP/PS1 mice showed reduced place cell pairwise reactivation but intact oscillations of slow wave sleep. a) *Spike time cross-correlations of 30 randomly selected place cells from one control and one APP/PS1 mouse, sorted by place field location on the track (colorbar). Grey line: coactivation.* ***b)*** *The percentage of place cell pairs that were temporally reactivated in slow wave sleep (SWS) was reduced in APP/PS1 compared to control mice, but not in quiet wakefulness (QW) or REM sleep (REMs).* ***c)*** *In SWS, power in the cortical slow oscillation, delta, spindle and hippocampal ripple bands was comparable between genotypes. Inset: cortical slow oscillation and delta power.* ***d)*** *Cortical spindle-triggered ripple power was comparable between genotypes. **$p < 0.01$, 2-sided t-tests. Control n=5 mice, 395 place cells, 2169 total cells; APP/PS1 n=6 mice, 237 place cells, 2133 total cells. Data are represented as mean ± S.E.M.*

To investigate possible mechanisms underlying reduced APP/PS1 place cell reactivation, we next evaluated the coordination of SWS hippocampal and cortical oscillations. Hippocampal SWRs, cortical spindles, cortical slow oscillations and their nested coordination are fundamental features of SWS that contribute to memory consolidation (49) (50). Whereas these SWS oscillations and

186 their coordination are degraded in Aβ plaque-laden AD models (20,22), before plaques
187 predominate we found that they remained intact. Specifically, SWR rates and duration (see above),
188 cortical SO power, cortical spindle power, and hippocampal ripple power ($p>0.05$, 2-sided t-tests,
189 Fig. 2c) were comparable between young APP/PS1 and control mice, and the coordination of
190 cortical spindles with hippocampal ripples was similar across genotypes ($p>0.05$, 2-sided t-test,
191 Fig. 2d). Thus, in contrast to impaired place cell pairwise reactivation at this early stage of Aβ
192 amyloidosis, the characteristic hippocampal and cortical oscillations of SWS remain intact.
193
194 **Impairment of online theta-gamma coupling before plaque deposition**
195 Since the physiological oscillations of SWS were intact in young APP/PS1 mice, we considered
196 the possibility that the reduction in place cell pairwise reactivation could be related to changes in
197 online oscillatory physiology linked to memory encoding. Intra-hippocampal and hippocampal-
198 cortical theta-gamma phase amplitude coupling (PAC) both contribute to memory encoding(13,24)
199 and degrade in Aβ plaque-bearing AD models (11,20,51–54). Whereas hippocampal theta and
200 gamma power were comparable across young APP/PS1 and control mice ($p>0.05$, 2-sided t-tests,
201 Fig 3a), intra-hippocampal theta (6-8 Hz) -gamma (40-80 Hz) PAC in APP/PS1 mice was impaired
202 ($p=0.03$, $T=2.3$, $df=13$, 2-sided t-test, Fig. 3b). Consistent with the possibility of accumulating
203 toxicity, hippocampal theta-gamma PAC in APP/PS1 mice was negatively correlated with age ($R=-$
204 0.7, $p=0.02$, Pearson correlation, Fig. 3c). These results were unchanged after controlling for the
205 possible contribution of theta harmonics (12) (Supplementary Fig. S4 a-c).
206
207 Cortical gamma power was also comparable between genotypes ($p>0.05$, 2-sided t-tests, Fig. 3d),
208 yet hippocampal theta (6-8 Hz) - cortical gamma (40-80 Hz) PAC was also impaired in young

209 APP/PS1 mice (p=0.02, T=2.5, df=13, 2-sided t-test, Fig. 3e). As with intrahippocampal theta-
210 gamma PAC, in APP/PS1 but not control mice, hippocampal-cortical PAC was negatively
211 correlated with age (R=-0.8, p=0.007, Pearson correlation, Fig. 3f), and these results persisted after
212 controlling for the possible contribution of theta harmonics (12) (Supplementary Fig. S4 d-f).
213 Together, these results suggest that accumulating APP degradation products degrade theta-gamma
214 PAC well before plaques robustly deposit.
215
216 Interestingly, the magnitude of hippocampal theta-gamma PAC in RUN was strongly correlated
217 with the extent of place cell pairwise reactivation in subsequent SWS in APP/PS1 mice (R=0.8,
218 p=0.02, Pearson correlation, Fig. 3g). In contrast, pairwise reactivation was not correlated with
219 age (p>0.05, Fig. 3h). These observations suggest that the impairment of theta-gamma PAC during
220 online behavior may serve as a proximal driver of the impairment of place cell pairwise
221 reactivation in SWS.
222
223 **Aberrant synchrony of somatic calcium fluctuations with hippocampal theta before plaque**
224 **deposition**
225 As oscillations both coordinate and reflect the coordination of neuronal activity, and as calcium
226 signaling links synaptic activity to synaptic plasticity and gene expression, we considered the
227 possibility that breakdown in the coordination of neuronal activity reflected in impaired theta-
228 gamma PAC might manifest at the cellular level in altered coordination of somatic calcium
229 fluctuations with the LFP. In exploratory behavior, neuronal calcium levels can synchronize with
230 theta oscillations, and this synchronization is aberrantly increased in Aβ plaque-laden mice (20).
231 We therefore measured the coherence of hippocampal neuronal calcium traces with the LFP in

232 APP/PS1 mice before significant plaque accumulation. Compared to control mice, APP/PS1 mice
233 showed hyper-synchronization of place cell calcium fluctuations with theta (repeated measures
234 ANOVA: F(3,16)=4.5, p=0.01, post-hoc comparison: control vs APP/PS1, place cells, p=0.02;
235 nonplace cells, p>0.05; Fig. 3i). Thus, at the pre-plaque stage preceding robust Aβ plaque
236 deposition, dysfunction of memory encoding processes manifest at both the oscillatory and the
237 cellular level.

238

239

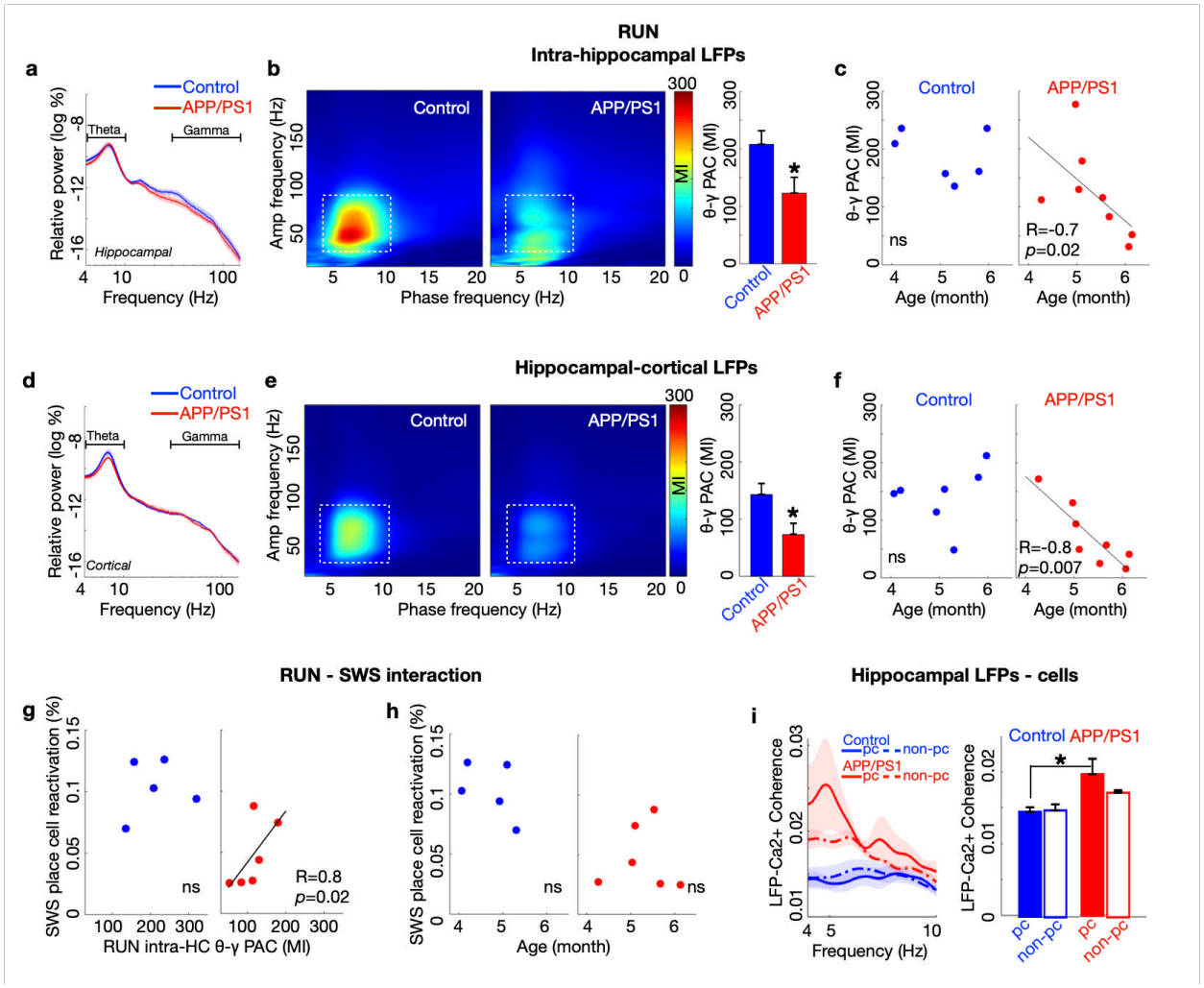

240

241 ***Figure 3. In pre-plaque APP/PS1 mice, theta-gamma phase-amplitude coupling in exploratory***
242 ***behavior was impaired and dynamic calcium fluctuations were excessively synchronized with***

hippocampal theta. a) *In RUN, hippocampal theta and gamma power in APP/PS1 and control mice were comparable.* ***b)*** *Intra-hippocampal theta (6-8Hz) - gamma (40-80Hz) phase - amplitude coupling (PAC) was reduced in APP/PS1 compared to control mice.* ***c)*** *Intrahippocampal theta-gamma PAC was negatively correlated with the age of APP/PS1 mice but not control mice.* ***d)*** *Cortical gamma power was comparable between genotypes.* ***e)*** *PAC of hippocampal theta (6-8Hz) - cortical gamma (40-80Hz) was reduced in APP/PS1 compared to control mice.* ***f)*** *The reduction of hippocampal theta- cortical gamma PAC was negatively correlated with age in APP/PS1 but not control mice.* ***g)*** *In APP/PS1 but not controls, the extent of place cell pairwise reactivation in SWS correlated with the magnitude of intra-hippocampal theta-gamma PAC in RUN.* ***h)*** *The proportion of reactivated place cell pairs in SWS was not correlated with age.* ***i)*** *Average theta-range LFP-cellular coherence of place cells was higher in APP/PS1 than control mice. *p < 0.05; b, e, 2 sided t-test; c, f, g, Pearson correlation; i, ANOVA with post-hoc comparisons. a –f: Control n=7 mice, APP/PS1 n=8 mice; g – i: Control n=5 mice, 395 place cells, 1774 non-place cells, 2169 total cells; APP/PS1 n=6 mice, 237 place cells, 1896 non-place cells, 2133 total cells. Data are represented as mean ± S.E.M. pc, place cells. Non-pc, nonplace cells.*

REM sleep theta-gamma coupling before plaque deposition

As intra-hippocampal and hippocampal-cortical theta-gamma PAC in REM sleep contribute to memory consolidation (55,56) and are diminished in Aβ plaque-bearing AD mice (20,53), we evaluated REM sleep theta-gamma PAC prior to robust Aβ plaque deposition. Hippocampal REM sleep theta and gamma power (p>0.05, 2-sided t-test, Fig. 4a), and intra-hippocampal theta (6-8 Hz) -gamma (40-80 Hz) PAC were comparable across genotypes (p>0.05, 2-sided t-test, Fig. 4b), consistent with prior results (53). Only a trend level correlation between intra-hippocampal PAC magnitude and the age of APP/PS1 mice was observed (R=-0.6, p=0.05, Pearson correlation, Fig. 4c), and this result did not survive after controlling for the possible contribution of theta harmonics (Supplementary Fig. S5 a-c).

REM sleep cortical gamma power (p>0.05, 2-sided t-test, Fig. 4d), and hippocampal theta (6-8 Hz) - cortical gamma (40-80 Hz) PAC were also comparable across genotypes (p>0.05, 2-sided t-test, Fig. 4e). Even so, in young APP/PS1 but not control mice, hippocampal-cortical PAC in REM

sleep was significantly and negatively correlated with age (R=-0.8, p=0.005, Pearson correlation, Fig. 4f), and this result persisted after controlling for the possible contribution of theta harmonics (Supplementary Fig. S5 d-f). These results suggest that as in exploratory behavior, theta-gamma PAC during REM sleep also falls with accumulation of toxic species before robust plaque deposition.

Because theta-gamma PAC in APP/PS1 mice was differentially affected in RUN and REM sleep but negatively correlated with age in both behavioral states, we compared theta-gamma PAC in RUN and REM sleep to one another. In both APP/PS1 and control mice, the magnitude of hippocampal theta - cortical gamma PAC in RUN and REM sleep were strongly correlated (Control R=0.9, p=0.001; APP/PS1 R=0.6, p=0.04; Pearson correlation, Fig 4h), with only a trend level correlation between intra-hippocampal theta-gamma PAC in RUN and REM sleep (Control R=0.6, p=0.05; APP/PS1 R=0.5, p=0.06; Pearson correlations, Fig. 4g).

We next sought to determine whether the hyper-synchronization of somatic calcium levels with the theta oscillation that we observed in exploratory behavior (Fig. 3i) extended to REM sleep. In contrast to findings in exploratory behavior, neuronal calcium synchronization with theta in REM sleep was similar across APP/PS1 and control mice (p>0.05, 2-sided t-tests, repeated measures ANOVA, Fig. 4i). These results suggest that hippocampal function in REM sleep may be more resilient than in other brain states to the accumulation of toxic APP cleavage products.

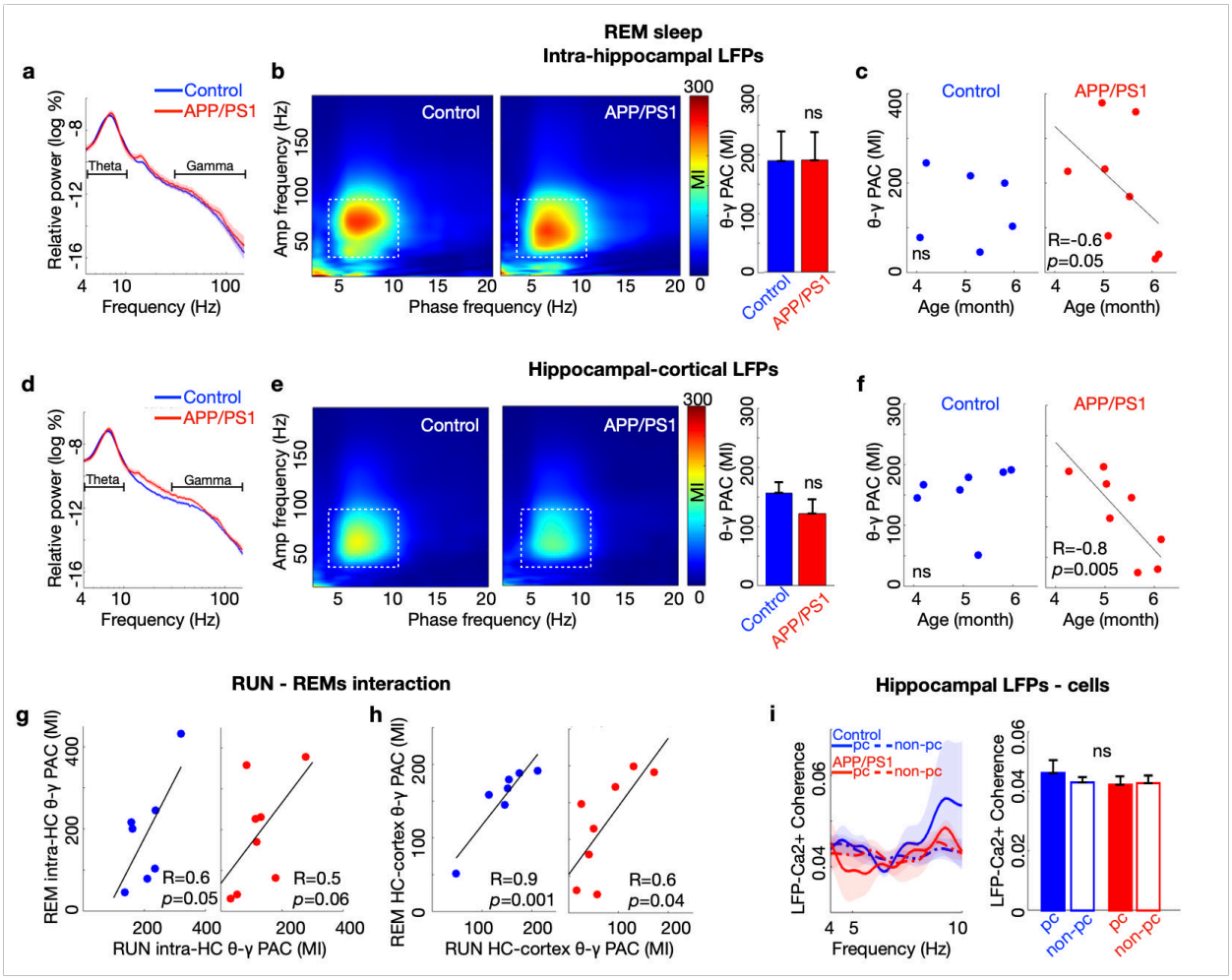

Figure 4. In young APP/PS1 mice, theta-gamma phase amplitude coupling in REM sleep was intact and correlated with theta-gamma phase-amplitude coupling during exploratory behavior. *__a__) In REM sleep, hippocampal spectral power, and __b)__ intra-hippocampal theta (6-8Hz) - gamma (40-80Hz) phase-amplitude coupling (PAC) were comparable in APP/PS1 and control mice. __c)__ Intrahippocampal theta-gamma PAC showed only a trending negative correlation with the age of APP/PS1 mice but not control mice. __d)__ Cortical spectral power, and __e)__ PAC of hippocampal theta (6-8Hz) - cortical gamma (40-80Hz) were comparable across genotypes. __f)__ Hippocampal theta-cortical gamma PAC was negatively correlated with age in APP/PS1 mice but not control mice. __g)__ Intra-hippocampal theta-gamma PAC between RUN and REM sleep showed a trending correlation in both genotypes. __h)__ Hippocampal theta - cortical gamma PAC in RUN and in REM sleep were significantly correlated in both AP/PS1 and control mice. __i)__ Average theta-range LFP-cellular coherence in REM sleep was comparable across APP/PS1 and control mice. b, e, 2 sided t-test; c, f, g, h, Pearson correlation; i, ANOVA with post-hoc comparisons. a – g: Control n=7 mice, APP/PS1 n=8 mice; i: Control n=5 mice, 395 place cells, 2169 total cells; APP/PS1 n=6 mice, 237 place cells, 2133 total cells. Data are represented as mean ± S.E.M. pc, place cells. Non-pc, nonplace cells.*

Discussion

In the context of well-described impairments of hippocampal neurophysiology in Aβ plaque-laden mice yet limited therapeutic benefits in manifest AD from targeting Aβ plaques, we investigated hippocampal functions that contribute to memory encoding and consolidation in young APP/PS1 mice harboring AD-associated gene mutations but lacking significant Aβ plaque burden. We found reduced theta-gamma PAC and excessive theta synchronization of hippocampal place cells with their surrounding LFP during exploratory behavior, and reduced place cell pairwise reactivation in subsequent SWS. These diverse impairments of neural functions underlying memory encoding and consolidation manifest before significant plaque burden and implicate other toxic processes in AD.

Hippocampal place cells encode the environment during online behavior, and their network reactivation during offline behaviors, including hippocampal replay during sharp wave ripples (46,57), contributes to sleep-dependent learning (46,58) and memory consolidation (47,59,60). Prior work has reported reduced place cell pairwise reactivation in Aβ plaque bearing mice (21), and the present results show that this result arises prior to significant Aβ plaque burden. The impairment of pairwise reactivation did not result from differences in behavior, LFP properties such as ripple rate and duration, or cellular properties such as calcium event rate between young APP/PS1 and control mice. Likewise, although the coordination of cortical slow oscillations, corticothalamic spindles, and hippocampal sharp wave ripples is a key feature of memory consolidation in SWS (49,50), and this coordination degrades in Aβ plaque-bearing animals (20,22), these oscillations and their coordination were preserved in young APP/PS1 mice lacking robust plaque deposits. As such, the reduced place cell pairwise reactivation observed in these mice stands in contrast with intact SWS oscillatory coordination.

Brain oscillations and their coupling play a crucial role in hippocampal-dependent memory functions. Online intra-hippocampal and hippocampal-cortical theta-gamma PACs have been linked to memory encoding (12–19), and, like the coordinated oscillations of SWS, are also impaired in multiple AD models harboring Aβ plaques (11,20,51–54). In contrast to the preserved oscillations of SWS, online hippocampal and hippocampal-cortical theta-gamma PACs were reduced in young APP/PS1 mice. As the extent of these reductions correlated with age, online theta-gamma PAC appears to degrade as APP degradation products such as soluble AβO accumulate.

The intra-hippocampal and hippocampal-cortical theta-gamma PACs of REM sleep have also been linked to memory consolidation (12,13) . While these deteriorate in plaque-laden AD model mice (20), the present findings show that before significant plaque deposition, theta-gamma PACs of REM sleep remain grossly preserved, consistent with prior results (22). Even so, a subtle vulnerability was evident, in that hippocampal-cortical theta-gamma PAC declined with increasing age.

In plaque-laden APP/PS1 mice, CA1 neuronal calcium fluctuations are excessively synchronized with hippocampal theta (20). Consistent with both this result and the greater vulnerability of online theta-gamma PAC compared to REM sleep in young APP/PS1 mice, hyper-synchronization of neuronal calcium oscillations with the hippocampal LFP was detected in young APP/PS1 mice in exploratory behavior alone. Although the mechanisms underlying impaired theta-gamma PAC and aberrant synchronization of neuronal calcium levels with the theta oscillation remain to be

determined, brain oscillations and their coupling are known to reflect the coordinated activity of large populations of excitatory and inhibitory neurons, and their imbalance or dyscoordination may contribute. In this context, it is possible that Aβ-mediated dysfunction of inhibitory neurons and their synapses may contribute to these findings (61).

Interestingly, despite the relatively small dataset, the degree of impairment of hippocampal theta-gamma PAC in exploratory behavior was correlated with the reduction of place cell pairwise reactivation in subsequent SWS. This observation raises the possibility of a primary deleterious effect of AβO or other APP degradation product on memory encoding online that then impairs memory consolidation in SWS. Linked impairments across behavioral states mediated by the effects of impaired theta-gamma PAC and hyper-synchronized neuronal calcium fluctuations on theta sequences that link the activity of adjacent place cells into trajectories within each theta cycle is one potential mechanism for this observation (62–64). This possibility will be worth assessing in future studies.

Although we observed marked abnormalities of hippocampal function across the sleep-wake cycle of young APP/PS1 mice, we did not detect aberrant neuronal hyperactivity, as has been reported in studies of anesthetized APP/PS1 mice (37–39). Instead, we observed a tendency towards hypoactivity in non-theta offline states. Reports of changes in neuronal activity in APP/PS1 mice have been heterogeneous (39), and prior work has shown that hyperactivity in young APP/PS1 mice is brought out by and depends on anesthesia (39). In this context, the present results suggest that hippocampal dynamic calcium hyperactivity in the behaving animal does not appear to be a prominent and requisite finding of early Aβ pathology.

382

383 Interestingly, the hippocampal systems level impairments observed here in young APP/PS1 mice
384 precede many of the behavioral impairments that arise in this AD model on standard behavioral
385 assays, although deficits of contextual memory have been reported to start around 6 months (65,66).
386 Thus, sampling hippocampal systems level function appears to provide a sensitive readout of brain
387 dysfunction in AD models.

388

389 While tau fibrils and neuronal loss are strong predictors of cognitive impairment in AD (67,68),
390 the current findings support the early contribution of additional AD-associated processes linked to
391 APP processing. Prior to plaque deposition, APP cleavage products including toxic soluble species
392 of Aβ accumulate. Among these, AβO are well-known to be cytotoxic and have been shown to
393 induce cognitive impairment (31,36,69). Among soluble Aβ species, small oligomers are
394 particularly toxic (36), and levels of small brain AβO but not monomer have been shown to
395 correlate with AD progression in APP/PS1 mice in the age range studied here (42).

396

397 Given the cellular and synaptic toxicity of AβO and their relevance to AD progression, as well as
398 the minimal levels of Aβ protofibrils detectable in young APP/PS1 mice (42), the accumulation of
399 AβO is well-positioned to contribute to the marked systems-level hippocampal dysfunctions
400 observed here. Even so, other non-Aβ mechanisms resulting from APP overexpression and the PS1
401 mutation (25,70) may also contribute. Among these, non-Aβ APP cleavage products such as
402 sAPPα, APP intracellular domain (AICD) and P3 fragment are biologically active (71,72), and
403 soluble APP products have been associated with cognitive impairment, neuronal loss,
404 electrophysiological abnormalities and GABA reduction (73). In addition, PS1 mutations through

405 their impact on γ-secretase function affect digestion of γ-secretase substrates including but not
406 limited to APP (74–76). Like the PS1dE9 mutation present in the APP/PS1 mouse (77), PS1
407 mutations typically reduce γ-secretase activity, leading to complex downstream effects including
408 altered calcium homeostasis (78), increased inflammatory responses in the brain (75), and
409 contributing to progressive brain atrophy, memory deficits, and synaptic impairments (75). Future
410 experiments to dissect the contributions of each potential mechanism to hippocampal systems
411 failure will be of value.
412
413 Strengths of this study include the use of a well-characterized, freely behaving AD model to
414 evaluate hippocampal functions underlying memory encoding and consolidation before Aβ
415 plaques predominate, free from the complexities associated with anesthesia. The acquisitions of
416 simultaneous dynamic calcium imaging and local electrophysiological recordings is a further
417 strength, enabling us to relate brain oscillations critical for normal hippocampal mnemonic
418 functions to neuronal calcium fluctuations, place cell activity, and their reactivation in SWS.
419 Limitations of this study include the use of a single model of amyloidosis, and additional work in
420 other models will be informative. A further limitation is the correlative nature of the work. In this
421 regard, future, causal experiments will prove useful to identify the factors underlying the
422 hippocampal physiological impairments observed here.
423
424 In summary, the results of this study in AD model mice prior to robust Aβ plaque deposition reveal
425 impairments in hippocampal cellular and oscillatory functions that contribute to both memory
426 encoding and consolidation. Targeting APP related cascades rather than Aβ plaques, per se, may

427 improve upon the significant but, to date, only modest effectiveness of anti-amyloid antibody
428 therapies for AD [1–4].
429
430 **Materials and Methods**
431 All procedures were approved by the Institutional Animal Care and Use Committees of the
432 Massachusetts General Hospital and followed the ethical guidelines of the US National Institutes
433 of Health.
434
435 **Surgical preparation**
436 All procedures were similar to our previous studies (20,79). Briefly, B6;C3-Tg (APPswe,
437 PSEN1dE9) 85Dbo/Mmjax transgenic mice (APP/PS1) mice (Jackson Laboratory) and their
438 age/gender matched non-transgenic control litters were firstly injected with 1 μL AAV-hSyn-
439 GCaMP6f-GFP into the hippocampal CA1 region (AP -2.1 mm, ML -1.65 mm, DV -1.4 mm)
440 under anesthesia (isoflurane 1.5-2%). Two weeks later, a grin lens (1 mm diameter, AP -2.1 mm,
441 ML -1.65 mm, DV -1.4 mm) and a custom drivable probe holding 7 stereotrodes (AP -2.8 mm,
442 ML 2.6 mm, -36 º relative to the AP axis, -39 º relative to the inter-aural axis; DV -1.2 mm) were
443 implanted ipsilaterally, to sample the LFP in the vicinity of the calcium imaging site, with
444 cerebellar ground. The microscope baseplate was attached three weeks later. Carprofen (10 mg/kg,
445 s.c) was used for postoperative analgesia. Animals were housed in individual cages with a 12 hr
446 light/12hr dark- standard light cycle. All mice were male to avoid sex differences in Aβ
447 pathogenesis in APP/PS1 mice (80).
448
449 **Calcium imaging and electrophysiology recordings**

450 The Inscopix^{TM} nVista3 mini-microscope and acquisition system were used to sample calcium
451 imaging at 20 Hz. Local field potential (LFP) (Neuralynx^{TM}) was sampled at 2 kHz followed by
452 0.5-900 Hz filtering. Animal position was recorded with overhead camera tracking of two LED
453 diodes mounted on the headstage. Electrophysiology and calcium imaging were acquired
454 simultaneously: Electrophysiology was recorded continuously, while calcium imaging was
455 recorded in 10 min acquisition blocks and 4-5 minute intervals off-camera to avoid photobleaching.
456 Recordings were synchronized and aligned by TTL pulses offline.
457
458 **Behavior and sleep stages**
459 Quiet wakefulness (QW), slow-wave sleep (SWS), and REM sleep were acquired immediately
460 after track sessions in the home cage within the same recording room. Exploratory behavior (RUN)
461 was defined when run velocity exceeded 1 cm/sec on the track; QW was defined as wakeful
462 immobility (< 0.5 cm/sec, eyes open) in the home cage; SWS was identified when SWRs were
463 present and delta/theta LFP power ratio exceeded 2, while the animal maintained a sleep posture;
464 REM sleep was identified when the theta/delta LFP power ratio exceeded 2 in sleep.
465
466 **Data analysis.** All analyses were performed using MATLAB (2019b) and were similar to our
467 previous studies (20,79).
468 *Calcium imaging:* Inscopix Data Processing Software (IDPS, Inscopix, Palo Alto, California) was
469 used for movie preprocessing, motion correction, normalization ΔF/F and constrained non-
470 negative matrix factorization (CNMFE) cell identification(81). The shape and signal-noise-ratio
471 (SNR) of each cell soma was reviewed manually for quality control. Calcium events were then
472 detected at 2 Z scores above the mean, with onset at 30% of peak amplitude. Low rate cells was

473 defined as < 0.25 transients/min (20,82); high rate cells was defined as > 2 Z scores above the
474 mean of the control group for each behavioral state (20).
475 *Place cell analyses:* Spatial tuning curves (3 cm bins) were constructed for each cell for each
476 running direction using all detected calcium events acquired during running. Spatial information
477 was computed and compared to 1000 shuffled spatial information distributions to test significance
478 (Monte Carlo p-value < 0.05) (83). Place field width was defined at 50% of peak firing distribution
479 over track location (84). Spike time cross-correlations of all place cell pairs in both online
480 (exploratory/RUN) and subsequent offline (QW, SWS) states were calculated. Reactivation was
481 defined when the same pair was coactivated during both online and specific offline states (48).
482 Coactivation was defined based on the distinguished clusters (cluster 1 not coactivated: <0.001,
483 and cluster 2 coactivated: >0.02) in the distribution of correlations of all place cell pairs in each
484 state (Fig. S2). Results persisted across a broad range of thresholds (between >0.001 and <0.02),
485 here we used >0.002 per previous work (48). Proportions of reactivated pairs among all pairs of
486 each animal were used to compare between genotypes. Recordings with at least 10 place cells (5
487 out of 7 control mice and 6 out of 8 APP/PS1 mice) were included in the pairwise reactivation
488 analysis.
489 *LFP analyses:* LFPs were filtered to obtain slow oscillations (0.5-1 Hz), delta (1-4 Hz), theta (4-
490 10 Hz), gamma (30-150 Hz), and ripples (100-300 Hz). The spectrograms of each channel were
491 calculated using the Chronux toolbox (85) with a moving window of size 2 s and step size 1 s. A
492 stereotrode in s. radiatum showing high amplitude theta was used for assessments of RUN and
493 REM sleep; a stereotrode in s. pyramidale showing high amplitude SWRs was used for
494 assessments of QW and SWS; a stereotrode within cortex showing slow oscillations and sleep
495 spindles was also used. Power spectra were computed from 0 to 200 Hz using the Chronux toolbox

496 (85), and the sum of relative power of each frequency band was used for quantification. Phase-
497 amplitude-coupling (PAC) modulation index (MI) was calculated with 1-25 Hz for phase
498 frequency and 1-300 Hz for amplitude frequency using the MATLAB toolbox
499 https://data.mrc.ox.ac.uk/data-set/matlab-toolbox-estimating-phase-amplitude-coupling (86,87),
500 and the mean value of the high coupling region was used for quantification (22). Spindle events
501 were detected at 1.25 Z score with minimum length of 200 ms; SWR events were detected at 3 Z
502 score with minimum length of 20 ms (49). LFPs were downsampled to the same sampling rate as
503 calcium imaging for the Chronux coherence analysis (85) for oscillatory-cellular synchronization
504 (20).
505
506 **Biochemistry**
507 *Brain protein extraction:* Mice were perfused with cold PBS containing protease inhibitor (cat #
508 A32957), and the brain was rapidly excised. One hemisphere was separated for
509 immunohistochemistry analyses. Cortex and hippocampus were dissected from the remaining
510 hemisphere and immediately frozen in liquid nitrogen, then stored at −80°C before use. Protein
511 extraction was performed as indicated by the ELISA kit. In summary, frozen brain samples were
512 homogenized in 10 vol (w/v) of cold TBS containing protease inhibitor using a Teflon-glass and
513 centrifuged at 16,000 x g for 30 min at 4°C. The pellets were re-suspended in TBS plus 1% Triton
514 X-100 containing protease inhibitor (TBS-T) and centrifuged at 16,000 x g for another 30 min at
515 4°C. The TBS-T fraction was used to measure oligomeric β-amyloid. The total protein
516 concentration in TBS-T fractions was measured using the BCA protein assay kit (cat# 23225).

517 *ELISA:* ELISA was used to quantify oligomeric β-amyloid in cortical and hippocampal samples
518 (Biosensis cat# BEK-2215-1P/2P). Oligomeric β-amyloid concentration was determined using a
519 standard curve, and values are reported as ng/mg of protein. Analyses were blinded to animal age.
520 *Immunohistochemistry:* Hemibrains were drop-fixed in 4% paraformaldehyde for two days and
521 sectioned at 40 mm on a vibratome (Leica, Buffalo Grove, IL). Sections were collected in a 1 in 4
522 series and stored in PBS at 4°C. Sections were mounted, and antigen retrieval was performed with
523 citrate buffer at 95°C for 30 min. Next, sections were blocked and permeabilized in TBS-T with
524 5% bovine serum albumin (BSA) and 5% normal goat serum (NGS) for 1h. Sections were
525 incubated overnight in Alexa Fluor 488 Conjugate primary β-Amyloid antibody (D54D2, cat#
526 51374S) at 4C. Following several washes in PBS, slides were cover slipped with anti-fade
527 mounting media, and images were acquired using an Olympus VS120 Slide Scanner.
528
529 **Statistical analysis**
530 All group values were represented as mean ± s.e.m. For analyses of dynamic calcium imaging
531 hypo- and hyperactivity, mixed effects models were used. For the remaining analyses, Student's
532 *t*-test and one-way ANOVA with repeated measures followed by *post hoc* tests were used for
533 statistical analyses according to the experimental design (SPSS). The significance threshold was
534 set at $p < 0.05$.
535
536 **Acknowledgements**
537 We thank Joseph J. Locascio for statistical consultation.
538

Funding disclosure

This work was supported by NIH grants to SNG (R01 AG054551; R01 AG077611).

Author contributions

Conceptualization, H.L., Z.Z. and S.N.G.; Methodology, H.L., Z.Z., A.F. and S.N.G.; Software, H.L. and S.N.G.; Validation, H.L., Z.Z., A.F., H.K.L. and R.J.G.; Formal Analysis, H.L.; Investigation, Z.Z., A.F., H.K.L. and R.J.G.; Resources, H.L., Z.Z., A.F., H.K.L. and R.J.G.; Data Curation, H.L. and R.J.G.; Writing – Original Draft, H.L. and S.N.G.; Writing – Review & Editing, H.L., Z.Z., A.F., H.K.L., R.J.G. and S.N.G.; Visualization, H.L.; Supervision, S.N.G.; Project Administration, S.N.G.; Funding Acquisition, S.N.G.

Competing interests

The authors declare no competing interests.

Data reporting

The datasets generated and analyzed in the current study are available in the Dryad repository, https://datadryad.org/stash/share/gN7A2L9rPMErDH74jxAWQUdjKm7A89v4ERaftNsJOiA

References

1. Bloom GS. Amyloid-β and Tau: The Trigger and Bullet in Alzheimer Disease Pathogenesis. JAMA Neurology. 2014 Apr 1;71(4):505–8.

2. van Dyck CH, Swanson CJ, Aisen P, Bateman RJ, Chen C, Gee M, et al. Lecanemab in Early Alzheimer's Disease. New England Journal of Medicine. 2023 Jan 5;388(1):9–21.

3. Mintun MA, Lo AC, Duggan Evans C, Wessels AM, Ardayfio PA, Andersen SW, et al. Donanemab in Early Alzheimer's Disease. N Engl J Med. 2021 May 6;384(18):1691–704.

4. Budd Haeberlein S, Aisen PS, Barkhof F, Chalkias S, Chen T, Cohen S, et al. Two Randomized Phase 3 Studies of Aducanumab in Early Alzheimer's Disease. J Prev Alzheimers Dis. 2022 Apr 1;9(2):197–210.

5. Honig LS, Vellas B, Woodward M, Boada M, Bullock R, Borrie M, et al. Trial of Solanezumab for Mild Dementia Due to Alzheimer's Disease. N Engl J Med. 2018 Jan 25;378(4):321–30.

6. Jankowsky JL, Fadale DJ, Anderson J, Xu GM, Gonzales V, Jenkins NA, et al. Mutant presenilins specifically elevate the levels of the 42 residue β-amyloid peptide in vivo: evidence for augmentation of a 42-specific γ secretase. Human Molecular Genetics. 2004 Jan 15;13(2):159–70.

7. Jankowsky JL, Slunt HH, Ratovitski T, Jenkins NA, Copeland NG, Borchelt DR. Co-expression of multiple transgenes in mouse CNS: a comparison of strategies. Biomol Eng. 2001 Jun;17(6):157–65.

8. O'Keefe J. Place units in the hippocampus of the freely moving rat. Experimental Neurology. 1976 Jan 1;51(1):78–109.

9. O'Keefe J, Burgess N, Donnett JG, Jeffery KJ, Maguire EA. Place cells, navigational accuracy, and the human hippocampus. Philos Trans R Soc Lond B Biol Sci. 1998 Aug 29;353(1373):1333–40.

10. Cacucci F, Yi M, Wills TJ, Chapman P, O'Keefe J. Place cell firing correlates with memory deficits and amyloid plaque burden in Tg2576 Alzheimer mouse model. Proceedings of the National Academy of Sciences. 2008 Jun 3;105(22):7863–8.

11. Mably AJ, Gereke BJ, Jones DT, Colgin LL. Impairments in spatial representations and rhythmic coordination of place cells in the 3xTg mouse model of Alzheimer's disease. Hippocampus. 2017;27(4):378–92.

12. Belluscio MA, Mizuseki K, Schmidt R, Kempter R, Buzsaki G. Cross-Frequency Phase-Phase Coupling between Theta and Gamma Oscillations in the Hippocampus. Journal of Neuroscience. 2012 Jan 11;32(2):423–35.

13. Colgin LL. Rhythms of the hippocampal network. Nat Rev Neurosci. 2016 Apr;17(4):239–49.

14. Jacobson TK, Howe MD, Schmidt B, Hinman JR, Escabí MA, Markus EJ. Hippocampal theta, gamma, and theta-gamma coupling: effects of aging, environmental change, and cholinergic activation. Journal of Neurophysiology. 2013 Apr;109(7):1852–65.

15. Kendrick KM, Zhan Y, Fischer H, Nicol AU, Zhang X, Feng J. Learning alters theta amplitude, theta-gamma coupling and neuronal synchronization in inferotemporal cortex. BMC Neuroscience. 2011 Jun 9;12(1):55.

16. Lisman JE, Jensen O. The Theta-Gamma Neural Code. Neuron. 2013 Mar 20;77(6):1002–16.

17. Tamura M, Spellman TJ, Rosen AM, Gogos JA, Gordon JA. Hippocampal-prefrontal theta-gamma coupling during performance of a spatial working memory task. Nat Commun. 2017 Dec 19;8(1):2182.

18. Tort ABL, Komorowski RW, Manns JR, Kopell NJ, Eichenbaum H. Theta–gamma coupling increases during the learning of item–context associations. Proc Natl Acad Sci USA. 2009 Dec 8;106(49):20942–7.

19. Vivekananda U, Bush D, Bisby JA, Baxendale S, Rodionov R, Diehl B, et al. Theta power and theta-gamma coupling support long-term spatial memory retrieval. Hippocampus. 2021;31(2):213–20.

20. Zhou H, Li H, Gowravaram N, Quan M, Kausar N, Gomperts SN. Disruption of hippocampal neuronal circuit function depends upon behavioral state in the APP/PS1 mouse model of Alzheimer's disease. Sci Rep. 2022 Dec 5;12(1):21022.

21. Prince SM, Paulson AL, Jeong N, Zhang L, Amigues S, Singer AC. Alzheimer's pathology causes impaired inhibitory connections and reactivation of spatial codes during spatial navigation. Cell Rep. 2021 Apr 20;35(3):109008.

22. Zhurakovskaya E, Ishchenko I, Gureviciene I, Aliev R, Gröhn O, Tanila H. Impaired hippocampal-cortical coupling but preserved local synchrony during sleep in APP/PS1 mice modeling Alzheimer's disease. Sci Rep. 2019 Dec;9(1):5380.

23. Buzsáki G. Theta Oscillations in the Hippocampus. Neuron. 2002 Jan;33(3):325–40.

24. Colgin LL. Theta–gamma coupling in the entorhinal–hippocampal system. Current Opinion in Neurobiology. 2015 Apr;31:45–50.

25. O'Brien RJ, Wong PC. Amyloid precursor protein processing and Alzheimer's disease. Annu Rev Neurosci. 2011;34:185–204.

26. Arbel-Ornath M, Hudry E, Boivin JR, Hashimoto T, Takeda S, Kuchibhotla KV, et al. Soluble oligomeric amyloid-β induces calcium dyshomeostasis that precedes synapse loss in the living mouse brain. Molecular Neurodegeneration. 2017 Mar 21;12(1):27.

626 27. Cleary JP, Walsh DM, Hofmeister JJ, Shankar GM, Kuskowski MA, Selkoe DJ, et al. Natural
627 oligomers of the amyloid-β protein specifically disrupt cognitive function. Nat Neurosci.
628 2005 Jan;8(1):79–84.

629 28. Cline EN, Bicca MA, Viola KL, Klein WL. The Amyloid-β Oligomer Hypothesis: Beginning
630 of the Third Decade. Perry G, Avila J, Moreira PI, Sorensen AA, Tabaton M, editors. JAD.
631 2018 Jun 12;64(s1):S567–610.

632 29. Ding Y, Zhao J, Zhang X, Wang S, Viola KL, Chow FE, et al. Amyloid Beta Oligomers
633 Target to Extracellular and Intracellular Neuronal Synaptic Proteins in Alzheimer's Disease.
634 Frontiers in Neurology [Internet]. 2019 [cited 2024 Jan 5];10. Available from:
635 https://www.frontiersin.org/articles/10.3389/fneur.2019.01140

636 30. Faucher P, Mons N, Micheau J, Louis C, Beracochea DJ. Hippocampal Injections of
637 Oligomeric Amyloid β-peptide (1–42) Induce Selective Working Memory Deficits and Long-
638 lasting Alterations of ERK Signaling Pathway. Frontiers in Aging Neuroscience [Internet].
639 2016 [cited 2023 Jun 16];7. Available from:
640 https://www.frontiersin.org/articles/10.3389/fnagi.2015.00245

641 31. Ferreira ST, Lourenco MV, Oliveira MM, De Felice FG. Soluble amyloid-β oligomers as
642 synaptotoxins leading to cognitive impairment in Alzheimer's disease. Front Cell Neurosci.
643 2015 May 26;9:191.

644 32. Nicole O, Hadzibegovic S, Gajda J, Bontempi B, Bem T, Meyrand P. Soluble amyloid beta
645 oligomers block the learning-induced increase in hippocampal sharp wave-ripple rate and
646 impair spatial memory formation. Sci Rep. 2016 Mar 7;6(1):22728.

647 33. Özcan GG, Lim S, Leighton PL, Allison WT, Rihel J. Sleep is bi-directionally modified by
648 amyloid beta oligomers. Sehgal A, Eisen MB, Musiek ES, editors. eLife. 2020 Jul
649 14;9:e53995.

650 34. Shankar GM, Li S, Mehta TH, Garcia-Munoz A, Shepardson NE, Smith I, et al. Amyloid-β
651 protein dimers isolated directly from Alzheimer's brains impair synaptic plasticity and
652 memory. Nat Med. 2008 Aug;14(8):837–42.

653 35. Malinow R, Malenka RC. AMPA receptor trafficking and synaptic plasticity. Annu Rev
654 Neurosci. 2002;25:103–26.

655 36. Yang T, Li S, Xu H, Walsh DM, Selkoe DJ. Large Soluble Oligomers of Amyloid β-Protein
656 from Alzheimer Brain Are Far Less Neuroactive Than the Smaller Oligomers to Which They
657 Dissociate. J Neurosci. 2017 Jan 4;37(1):152–63.

658 37. Busche MA, Chen X, Henning HA, Reichwald J, Staufenbiel M, Sakmann B, et al. Critical
659 role of soluble amyloid-β for early hippocampal hyperactivity in a mouse model of
660 Alzheimer's disease. Proc Natl Acad Sci USA. 2012 May 29;109(22):8740–5.

661 38. Busche MA, Konnerth A. Neuronal hyperactivity – A key defect in Alzheimer's disease?
662 BioEssays. 2015;37(6):624–32.

39. Zarhin D, Atsmon R, Ruggiero A, Baeloha H, Shoob S, Scharf O, et al. Disrupted neural correlates of anesthesia and sleep reveal early circuit dysfunctions in Alzheimer models. Cell Reports. 2022 Jan;38(3):110268.

40. Garcia-Alloza M, Robbins EM, Zhang-Nunes SX, Purcell SM, Betensky RA, Raju S, et al. Characterization of amyloid deposition in the APPswe/PS1dE9 mouse model of Alzheimer disease. Neurobiol Dis. 2006 Dec;24(3):516–24.

41. Takeda S, Hashimoto T, Roe AD, Hori Y, Spires-Jones TL, Hyman BT. Brain interstitial oligomeric amyloid β increases with age and is resistant to clearance from brain in a mouse model of Alzheimer's disease. FASEB J. 2013 Aug;27(8):3239–48.

42. Zhang L, Yang C, Li Y, Niu S, Liang X, Zhang Z, et al. Dynamic Changes in the Levels of Amyloid-β42 Species in the Brain and Periphery of APP/PS1 Mice and Their Significance for Alzheimer's Disease. Front Mol Neurosci. 2021 Aug 27;14:723317.

43. Webster SJ, Bachstetter AD, Van Eldik LJ. Comprehensive behavioral characterization of an APP/PS-1 double knock-in mouse model of Alzheimer's disease. Alzheimers Res Ther. 2013 May 24;5(3):28.

44. Knierim JJ, Kudrimoti HS, McNaughton BL. Place cells, head direction cells, and the learning of landmark stability. J Neurosci. 1995 Mar;15(3 Pt 1):1648–59.

45. Jun H, Bramian A, Soma S, Saito T, Saido TC, Igarashi KM. Disrupted Place Cell Remapping and Impaired Grid Cells in a Knockin Model of Alzheimer's Disease. Neuron. 2020 Sep 23;107(6):1095-1112.e6.

46. Ego-Stengel V, Wilson MA. Disruption of ripple-associated hippocampal activity during rest impairs spatial learning in the rat. Hippocampus. 2010;20(1):1–10.

47. Ólafsdóttir HF, Bush D, Barry C. The Role of Hippocampal Replay in Memory and Planning. Curr Biol. 2018 Jan 8;28(1):R37–50.

48. Wilson MA, McNaughton BL. Reactivation of Hippocampal Ensemble Memories During Sleep. Science. 1994 Jul 29;265(5172):676–9.

49. Siapas AG, Wilson MA. Coordinated Interactions between Hippocampal Ripples and Cortical Spindles during Slow-Wave Sleep. Neuron. 1998 Nov;21(5):1123–8.

50. Born J, Rasch B, Gais S. Sleep to Remember. Neuroscientist. 2006 Oct 1;12(5):410–24.

51. Bazzigaluppi P, Beckett TL, Koletar MM, Lai AY, Joo IL, Brown ME, et al. Early-stage attenuation of phase-amplitude coupling in the hippocampus and medial prefrontal cortex in a transgenic rat model of Alzheimer's disease. Journal of Neurochemistry. 2018;144(5):669–79.

52. Etter G, van der Veldt S, Manseau F, Zarrinkoub I, Trillaud-Doppia E, Williams S. Optogenetic gamma stimulation rescues memory impairments in an Alzheimer's disease mouse model. Nat Commun. 2019 Dec;10(1):5322.

53. Gurevicius K, Lipponen A, Tanila H. Increased Cortical and Thalamic Excitability in Freely Moving APPswe/PS1dE9 Mice Modeling Epileptic Activity Associated with Alzheimer's Disease. Cerebral Cortex. 2013 May;23(5):1148–58.

54. Stoiljkovic M, Kelley C, Stutz B, Horvath TL, Hajós M. Altered Cortical and Hippocampal Excitability in TgF344-AD Rats Modeling Alzheimer's Disease Pathology. Cerebral Cortex. 2019 Jun 1;29(6):2716–27.

55. Bandarabadi M, Boyce R, Gutierrez Herrera C, Bassetti CL, Williams S, Schindler K, et al. Dynamic modulation of theta-gamma coupling during rapid eye movement sleep. Sleep. 2019 Dec 24;42(12):zsz182.

56. Montgomery SM, Sirota A, Buzsáki G. Theta and Gamma Coordination of Hippocampal Networks during Waking and Rapid Eye Movement Sleep. J Neurosci. 2008 Jun 25;28(26):6731–41.

57. Joo HR, Frank LM. The hippocampal sharp wave-ripple in memory retrieval for immediate use and consolidation. Nat Rev Neurosci. 2018 Dec;19(12):744–57.

58. Girardeau G, Cei A, Zugaro M. Learning-Induced Plasticity Regulates Hippocampal Sharp Wave-Ripple Drive. J Neurosci. 2014 Apr 9;34(15):5176–83.

59. Atherton LA, Dupret D, Mellor JR. Memory trace replay: the shaping of memory consolidation by neuromodulation. Trends Neurosci. 2015 Sep;38(9):560–70.

60. Louie K, Wilson MA. Temporally Structured Replay of Awake Hippocampal Ensemble Activity during Rapid Eye Movement Sleep. Neuron. 2001 Jan;29(1):145–56.

61. Kurucu H, Colom-Cadena M, Davies C, Wilkins L, King D, Rose J, et al. Inhibitory synapse loss and accumulation of amyloid beta in inhibitory presynaptic terminals in Alzheimer's disease. European Journal of Neurology. 2022;29(5):1311–23.

62. Tang W, Jadhav SP. Multiple-Timescale Representations of Space: Linking Memory to Navigation. Annu Rev Neurosci. 2022 Jul 8;45:1–21.

63. Lisman J. The theta/gamma discrete phase code occuring during the hippocampal phase precession may be a more general brain coding scheme. Hippocampus. 2005;15(7):913–22.

64. Skaggs WE, McNaughton BL, Wilson MA, Barnes CA. Theta phase precession in hippocampal neuronal populations and the compression of temporal sequences. Hippocampus. 1996;6(2):149–72.

729 65. Lonnemann N, Korte M, Hosseini S. Repeated performance of spatial memory tasks
730 ameliorates cognitive decline in APP/PS1 mice. Behavioural Brain Research. 2023 Feb
731 13;438:114218.

732 66. Kilgore M, Miller CA, Fass DM, Hennig KM, Haggarty SJ, Sweatt JD, et al. Inhibitors of
733 Class 1 Histone Deacetylases Reverse Contextual Memory Deficits in a Mouse Model of
734 Alzheimer's Disease. Neuropsychopharmacology. 2010 Mar;35(4):870–80.

735 67. Medeiros R, Baglietto-Vargas D, LaFerla FM. The role of tau in Alzheimer's disease and
736 related disorders. CNS Neurosci Ther. 2011 Oct;17(5):514–24.

737 68. Niikura T, Tajima H, Kita Y. Neuronal Cell Death in Alzheimer's Disease and a
738 Neuroprotective Factor, Humanin. Curr Neuropharmacol. 2006 Apr;4(2):139–47.

739 69. Lambert MP, Barlow AK, Chromy BA, Edwards C, Freed R, Liosatos M, et al. Diffusible,
740 nonfibrillar ligands derived from Abeta1-42 are potent central nervous system neurotoxins.
741 Proc Natl Acad Sci U S A. 1998 May 26;95(11):6448–53.

742 70. Hampel H, Hardy J, Blennow K, Chen C, Perry G, Kim SH, et al. The Amyloid-β Pathway in
743 Alzheimer's Disease. Mol Psychiatry. 2021 Oct;26(10):5481–503.

744 71. Chow VW, Mattson MP, Wong PC, Gleichmann M. An Overview of APP Processing
745 Enzymes and Products. Neuromolecular Med. 2010 Mar;12(1):1–12.

746 72. Bukhari H, Glotzbach A, Kolbe K, Leonhardt G, Loosse C, Müller T. Small things matter:
747 Implications of APP intracellular domain AICD nuclear signaling in the progression and
748 pathogenesis of Alzheimer's disease. Prog Neurobiol. 2017 Sep;156:189–213.

749 73. Kreis A, Desloovere J, Suelves N, Pierrot N, Yerna X, Issa F, et al. Overexpression of wild-
750 type human amyloid precursor protein alters GABAergic transmission. Sci Rep. 2021 Sep
751 2;11(1):17600.

752 74. Do HN, Devkota S, Bhattarai A, Wolfe MS, Miao Y. Effects of presenilin-1 familial
753 Alzheimer's disease mutations on γ-secretase activation for cleavage of amyloid precursor
754 protein. Commun Biol. 2023 Feb 14;6(1):1–14.

755 75. Soto-Faguás CM, Sanchez-Molina P, Saura CA. Loss of presenilin function enhances tau
756 phosphorylation and aggregation in mice. Acta Neuropathol Commun. 2021 Sep 30;9:162.

757 76. Kelleher RJ, Shen J. Presenilin-1 mutations and Alzheimer's disease. Proc Natl Acad Sci U S
758 A. 2017 Jan 24;114(4):629–31.

759 77. Woodruff G, Young JE, Martinez FJ, Buen F, Gore A, Kinaga J, et al. The Presenilin-1 ΔE9
760 mutation results in reduced γ-secretase activity, but not total loss of PS1 function, in isogenic
761 human stem cells. Cell Rep. 2013 Nov 27;5(4):10.1016/j.celrep.2013.10.018.

762 78. Bagaria J, Bagyinszky E, An SSA. Genetics, Functions, and Clinical Impact of Presenilin-1
763 (PSEN1) Gene. Int J Mol Sci. 2022 Sep 19;23(18):10970.

79. Zhou H, Neville KR, Goldstein N, Kabu S, Kausar N, Ye R, et al. Cholinergic modulation of hippocampal calcium activity across the sleep-wake cycle. Colgin L, Frank MJ, editors. eLife. 2019 Mar 7;8:e39777.

80. Li X, Feng Y, Wu W, Zhao J, Fu C, Li Y, et al. Sex differences between APPswePS1dE9 mice in A-beta accumulation and pancreatic islet function during the development of Alzheimer's disease. Lab Anim. 2016 Aug 1;50(4):275–85.

81. Zhou P, Resendez SL, Rodriguez-Romaguera J, Jimenez JC, Neufeld SQ, Giovannucci A, et al. Efficient and accurate extraction of in vivo calcium signals from microendoscopic video data. Van Essen DC, editor. eLife. 2018 Feb 22;7:e28728.

82. Lerdkrai C, Asavapanumas N, Brawek B, Kovalchuk Y, Mojtahedi N, Olmedillas del Moral M, et al. Intracellular Ca^{2+} stores control in vivo neuronal hyperactivity in a mouse model of Alzheimer's disease. Proc Natl Acad Sci USA [Internet]. 2018 Feb 6 [cited 2022 Oct 27];115(6). Available from: https://pnas.org/doi/full/10.1073/pnas.1714409115

83. Markus EJ, Barnes CA, McNaughton BL, Gladden VL, Skaggs WE. Spatial information content and reliability of hippocampal CA1 neurons: Effects of visual input. Hippocampus. 1994 Aug;4(4):410–21.

84. Go MA, Rogers J, Gava GP, Davey CE, Prado S, Liu Y, et al. Place Cells in Head-Fixed Mice Navigating a Floating Real-World Environment. Frontiers in Cellular Neuroscience [Internet]. 2021 [cited 2023 Sep 14];15. Available from: https://www.frontiersin.org/articles/10.3389/fncel.2021.618658

85. Bokil H, Andrews P, Kulkarni JE, Mehta S, Mitra PP. Chronux: A platform for analyzing neural signals. Journal of Neuroscience Methods. 2010 Sep;192(1):146–51.

86. Onslow ACE, Bogacz R, Jones MW. Quantifying phase–amplitude coupling in neuronal network oscillations. Progress in Biophysics and Molecular Biology. 2011 Mar;105(1–2):49–57.

87. Osipova D, Hermes D, Jensen O. Gamma Power Is Phase-Locked to Posterior Alpha Activity. Rustichini A, editor. PLoS ONE. 2008 Dec 22;3(12):e3990.